Measurement of the cross section of e + e − → ηπ + π − at center-of-mass energies from 3.872 GeV to 4.700 GeV

BESIII Collaboration; Kalantar-Nayestanaki, N.; Kappert, R.; Rodin, V.

Published in:
Journal of High Energy Physics

DOI:
10.1007/JHEP12(2022)153

Publication date:
2022

Published for SISSA by Springer

Received: *March 11, 2022*
Revised: *May 25, 2022*
Accepted: *December 5, 2022*
Published: *December 27, 2022*

JHEP12(2022)153

Measurement of the cross section of $e^+e^- \to \eta\pi^+\pi^-$ at center-of-mass energies from 3.872 GeV to 4.700 GeV

The BESIII collaboration

E-mail: besiii-publications@ihep.ac.cn

Abstract: Using data samples with an integrated luminosity of 19 fb^{-1} at twenty-eight center-of-mass energies from 3.872 GeV to 4.700 GeV collected with the BESIII detector at the BEPCII electron-positron collider, the process $e^+e^- \to \eta\pi^+\pi^-$ and the intermediate process $e^+e^- \to \eta\rho^0$ are studied for the first time. The Born cross sections are measured. No significant resonance structure is observed in the cross section lineshape.

Keywords: Charm Physics, e^+-e^- Experiments

ArXiv ePrint: 2202.12748

https://doi.org/10.1007/JHEP12(2022)153

Contents

JHEP12(2022)153

1 Introduction

Since the discovery of the charmonium-like state $\chi_{c1}(3872)$ by Belle [1], a series of states, such as $Y(4260)$ [2] and $Z_c(3900)$ [3, 4], which are unexpected in charmonium spectroscopy, have been found. The $Y(4260)$ was observed by the BaBar Collaboration in $e^+e^- \to \gamma_{\rm ISR}\pi^+\pi^- J/\psi$, where the subscript ISR stands for initial state radiation, and confirmed by CLEO and Belle [5, 6]. In 2017, the BESIII Collaboration performed a dedicated scan of the process $e^+e^- \to \pi^+\pi^- J/\psi$ at center-of-mass (c.m.) energies $\sqrt{s}$ from 3.77 to 4.60 GeV. Two structures were observed with masses of $M = 4222.0 \pm 3.1 \pm 1.4\,{\rm MeV}/c^2$ and $M = 4320.0 \pm 10.4 \pm 7.0\,{\rm MeV}/c^2$ [7]. The former one was regarded as the previously observed $Y(4260)$, which was renamed to $Y(4220)$. The $Y(4220)$ state was confirmed by Born cross section measurements of the final states $\omega\chi_{c0}$ [8], $\pi^+\pi^- h_c$ [9], $\pi^+\pi^-\psi(3686)$ [10], and $\pi^+ D^0 D^{*-}$ [11] by BESIII.

The currently known decays of $Y(4220)$ occur only to open or hidden-charm final states. However, some related theories point out that charmonium-like states are also likely to decay to light hadron final states [12], shedding further light on the $Y(4220)$ [13]. Several measurements of the cross sections for e^+e^- annihilations to light hadrons have been measured by the BESIII Collaboration, such as $e^+e^- \to K^0_S K^\pm\pi^\mp\pi^0$ [14], $K^0_S K^\pm\pi^\mp$ [15], $p\bar{n}K^0_S K^- + c.c.$ [16], $p\bar{p}\pi^0$ [17] etc., but no significant structures have been found so far. In

order to better understand the composition and properties of the charmonium-like states, further searches for their decays to charmless light-hadron final states are important.

In this paper, we present the measurements of the Born cross section of the process $e^+e^- \to \eta\pi^+\pi^-$ at center-of-mass energies from 3.872 GeV to 4.700 GeV, and search for possible charmonium (ψ) or vector charmonium-like (Y) states in the corresponding lineshape.

2 BESIII detector and data sets

The BESIII detector is a magnetic spectrometer [18] located at the Beijing Electron Positron Collider (BEPCII). The cylindrical core of the BESIII detector consists of a helium-based multilayer drift chamber (MDC), a plastic scintillator time-of-flight system (TOF), and a CsI (Tl) electromagnetic calorimeter (EMC), which are all enclosed in a superconducting solenoidal magnet providing a 1.0 T magnetic field. The solenoid is supported by an octagonal flux-return yoke with resistive plate counter muon identifier modules interleaved with steel. The acceptance of charged particles and photons is 93% over 4π solid angle. The charged-particle momentum resolution at 1 GeV/c is 0.5%, and the specific ionization energy loss (dE/dx) resolution is 6% for the electrons from Bhabha scattering. The EMC measures photon energies with a resolution of 2.5% (5%) at 1 GeV in the barrel (end cap) region. The time resolution of the TOF barrel part is 68 ps, while that of the end cap part is 110 ps. The end cap TOF system was upgraded in 2015 with multi-gap resistive plate chamber technology, providing a time resolution of 60 ps [19, 20]. Muons with momentum above 0.5 GeV/c are identified by the iron flux return of the magnet instrumented with about 1272 m^2 of resistive plate muon counters (MuC) arranged in nine (eight) layers in the barrel (endcaps). The spatial resolution in the MuC is better than 2 cm.

The twenty-eight data sets taken at $\sqrt{s} = 3.872 \sim 4.700$ GeV are used in this analysis. The nominal energy of each data set is calibrated by the process $e^+e^- \to (\gamma_{\rm ISR/FSR})\mu^+\mu^-$ [21, 22], where the subscript FSR stands for final-state radiation. The integrated luminosity $\mathcal{L}$ is determined by large angle Bhabha events [23, 24], and the total integrated luminosity is approximately 19 fb^{-1}.

3 Monte Carlo simulation

Simulated data samples produced with GEANT4-based [25] Monte Carlo (MC) software, which includes the geometric description of the BESIII detector and the detector response, are used to determine detection efficiencies and to estimate background contributions. The simulation models the beam energy spread and ISR in the e^+e^- annihilations with the generator KKMC [26]. The inclusive MC simulation sample includes the production of open charm processes, the ISR production of vector charmonium(-like) states, and the continuum processes incorporated in KKMC. The known decay modes are modeled with EVTGEN [27] using branching fractions taken from the Particle Data Group (PDG) [28], and the remaining unknown ψ decays are modeled with LUNDCHARM [29]. The FSR from charged final state particles is incorporated using PHOTOS [30].

JHEP12(2022)153

In the signal MC simulation samples at each c.m. energy point, three exclusive processes are involved, which are the three-body non-resonant process $e^+e^- \to \eta\pi^+\pi^-$, and the two-body resonant processes, $e^+e^- \to a_2^{\pm}(1320)\pi^{\mp}$ and $\eta\rho^0$ [31]. The last process is simulated by the HELAMP model [27] following the dynamics of other vector charmonium decays, while the first two processes are simulated by phase space (PHSP) models. In determining the resulting detection efficiencies, the interference between $\eta\rho$ process and the three-body non-resonant process is included, while the interference between $a_2(1320)\pi$ process and the three-body non-resonant process is neglected due to the small event sample. The resulting detection efficiency is obtained by mixing the three processes weighted according to the number of observed events ($N_{\rm obs}$) and detection efficiency (ϵ).

4 Event selection

The charged tracks detected in the MDC are required to be within a polar angle (θ) range of $|\cos\theta| < 0.93$, where θ is the polar angle with the z-axis, which is the symmetry axis of the MDC. All the charged tracks are required to originate from the interaction region $V_{xy} < 1$ cm and $|V_z| < 10$ cm, where V_{xy} and $|V_z|$ are the distances of closest approach of the charged track to the collision vertex in the xy-plane and z direction, respectively.

Particle identification (PID) for charged tracks combines measurements of dE/dx in the MDC and the flight time in the TOF to form likelihoods $\mathcal{L}(h)$ for each hadron $h = p, K, \pi$ hypothesis. Tracks are identified as pions when the pion hypothesis has the greatest likelihood ($\mathcal{L}(\pi) > \mathcal{L}(K)$ and $\mathcal{L}(\pi) > \mathcal{L}(p)$).

Photon candidates are identified using showers in the EMC. The deposited energy of each shower must be more than 25 MeV in the barrel region ($|\cos\theta| < 0.80$) and more than 50 MeV in the end cap region ($0.86 < |\cos\theta| < 0.92$). To exclude showers that originate from charged tracks, the angle between the position of each shower in the EMC and the closest extrapolated charged track must be greater than 10 degrees. To suppress electronic noise and showers unrelated to the event, the difference between the EMC time and the event start time is required to be within [0,700] ns. Candidate events must have two charged tracks with zero net charge, and the number of photons should be 2 or greater. The two charged tracks must be identified as pions.

To improve the momentum and energy resolution and suppress the potential background contributions, a four-constraint (4C) kinematic fit, which constrains the total four-momentum of the final state particles to that of the initial colliding beams, is applied to the event under the hypothesis of $e^+e^- \to \gamma\gamma\pi^+\pi^-$. If more than one candidate (37% of the selected events) exists in an event, that with the smallest χ^2_{4C} is selected.

Potential background contributions are investigated with six equivalent-luminosity inclusive MC samples generated at c.m. energies from 4.009 GeV to 4.600 GeV, using an event-type analysis tool, TopoAna [32]. It is found that the main background contributions come from $e^+e^- \to \gamma\pi^+\pi^-$, $\mu^+\mu^-$, $\gamma\gamma e^+e^-$ and $e^+e^- \to J/\psi + \text{anything}$, $J/\psi \to hh$ or ll ($h = p, \pi$, $l = e, \mu$) processes. In the first background channel, a reconstructed photon e.g. from beam-related background is combined with the real photon to form a fake η signal. This background is suppressed by requiring the ratio $R = \frac{|E_{\gamma_1} - E_{\gamma_2}|}{p_\eta} < 0.90$, where $E_{\gamma_1}, E_{\gamma_2}$

JHEP12(2022)153

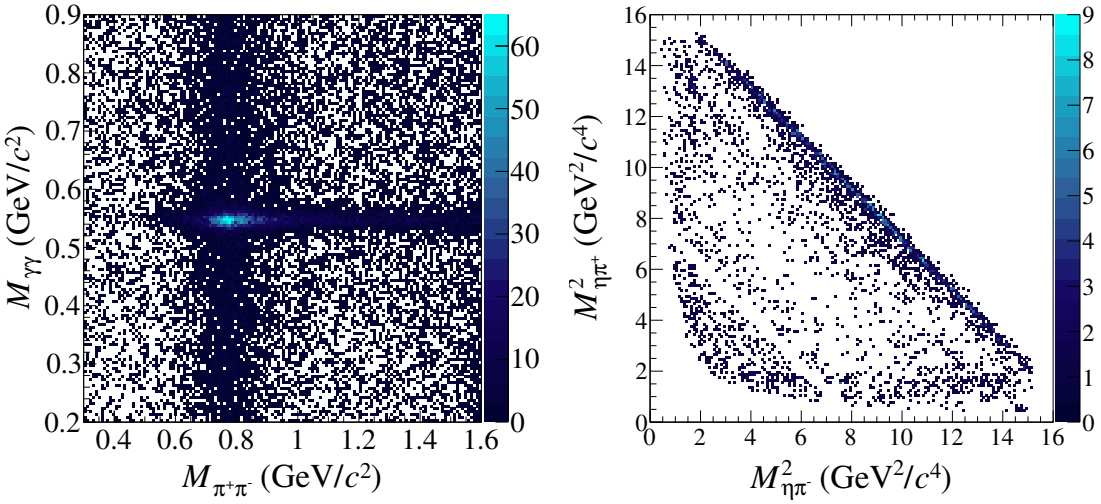

Figure 1. (left) Two-dimensional distributions of $M_{\gamma\gamma}$ versus $M_{\pi^+\pi^-}$ for the candidate events for all energy points, and (right) Dalitz plot in the η signal range with the selected events for the energy point at $\sqrt{s} = 4.180\,\text{GeV}$. The diagonal band without events in the Dalitz plot is due to the J/ψ-related event veto.

are the energies of the two photons from the fake η decay and p_η is the momentum of the fake η. The second background channel is suppressed by requiring the penetration hit depth in the MuC of charged track to be less than 40 cm since muons have penetration deeper hit depth. The third background channel is suppressed by requiring E/cp <0.7. Here, E and p denote the deposited energy in the EMC and the momentum of the charged track, respectively. The background from J/ψ-related events is vetoed by requiring the invariant mass of $\pi^+\pi^-$ not to fall into the J/ψ mass region [3.05, 3.15] GeV/c^2. Finally, it is found that the dominant remaining background channel is $e^+e^- \to \mu^+\mu^-$ due to $\mu - \pi$ misidentification since muons have higher penetration and therefore larger hit depth.

With the above selection criteria, there are significant enhancements close to the η and ρ^0 nominal masses in the two dimensional distribution of the invariant mass of $\gamma\gamma$ ($M_{\gamma\gamma}$) and $\pi^+\pi^-$ ($M_{\pi^+\pi^-}$), as can be seen in figure 1 (left). The η signal region is defined as $0.513 < M_{\gamma\gamma} < 0.581\,\text{GeV}/c^2$, and the lower and upper side-band regions are defined as $0.309 < M_{\gamma\gamma} < 0.445\,\text{GeV}/c^2$ and $0.649 < M_{\gamma\gamma} < 0.785\,\text{GeV}/c^2$, respectively. Figure 1 (right) shows the Dalitz plot of $M^2_{\eta\pi^+}$ versus $M^2_{\eta\pi^-}$ of events in the η signal region at $\sqrt{s} = 4.180\,\text{GeV}$. A clear ρ^0 band is seen, and the horizontal and vertical bands around $1.75\,\text{GeV}^2/c^4$ correspond to $e^+e^- \to a_2(1302)^\pm\pi^\mp$.

5 Signal yields

The η signal yields are obtained with unbinned likelihood fits to the $M_{\gamma\gamma}$ spectra. The signal function is described as a MC-simulated shape convolved with a Gaussian function to account for the difference of the detector resolutions between data and MC simulation, while the background function is described by a second-order Chebyshev polynomials. Figure 2(a) shows the fit result for all energy points combined.

JHEP12(2022)153

The $\eta\rho^0$ signal yields are obtained with a simultaneous unbinned likelihood fit to the $M_{\pi^+\pi^-}$ spectra of the events in the η signal region at all energy points. The ρ^0 resonance is parameterized by a Breit-Wigner (BW) propagator using the Gounaris-Sakurai (GS) model [33]. The parameterized propagator function is expressed as:

$$\mathrm{BW}^{\mathrm{GS}}(m) = \frac{1 + d(M)\Gamma/M}{M^2 - m^2 + f(m, M, \Gamma) - iM\Gamma(m, M, \Gamma)}, \tag{5.1}$$

with

$$\begin{aligned}
\Gamma(m, M, \Gamma) &= \Gamma \frac{m^2}{M^2} \left(\frac{\beta_\pi(m)}{\beta_\pi(M)}\right)^3, \\
d(M) &= \frac{3}{\pi}\frac{M_\pi^2}{k^2(M)} \ln\left(\frac{M + 2k(M)}{2M_\pi}\right) + \frac{M}{2\pi k(M)} - \frac{M_\pi^2 M}{\pi k^3(M)}, \\
f(m, M, \Gamma) &= \frac{\Gamma M^2}{k^3(M)}[k^2(m)(h(m) - h(M)) + (M^2 - m^2)k^2(M)h'(M)],
\end{aligned} \tag{5.2}$$

where

$$\begin{aligned}
\beta_\pi(m) &= \sqrt{1 - 4M_\pi^2/m^2}, \\
k(m) &= \frac{1}{2} m \beta_\pi(m), \\
h(m) &= \frac{2}{\pi}\frac{k(m)}{m} \ln\left(\frac{m + 2k(m)}{2M_\pi}\right),
\end{aligned} \tag{5.3}$$

and $h'(m)$ is the derivative of $h(m)$, m is the invariant mass of $\pi^+\pi^-$, M_π is the invariant mass of the π meson, and M and Γ are the mass and width of the ρ. The signal function is described by a coherent probability density function (PDF):

$$\mathrm{PDF}(m) = |\mathrm{BW}^{\mathrm{GS}}(m) + A \times \mathrm{Poly}_{\mathrm{PHSP}} \times e^{i\varphi}|^2, \tag{5.4}$$

where φ is the relative phase between the ρ and PHSP amplitudes, $\mathrm{Poly}_{\mathrm{PHSP}}$ is the PHSP amplitude contribution, which describes the non-ρ mode and is parameterized with a polynomial, and the parameter A is the normalization factor. The parameters of the signal function are left free in the fit. The non-η background shape is obtained by the normalized η side-bands summed over all energies. The number of background events is fixed to $f \cdot N_{\mathrm{sb}}$, where $f = 0.25$ is the scale factor since the non-η background shape is a linear one and the side-band region is two times wider than the signal region. The parameter N_{sb} is the number of side-band background events at each c.m. energy point. The fits at each point share the parameters of the signal function (eq. (5.4)). Figure 2(b) shows the fit result for the sum of all energy points.

The $a_2(1320)$ signal yield is obtained by a binned likelihood fit to the invariant mass of $\eta\pi^\pm$ ($M_{\eta\pi^\pm}$) spectrum summed over all energy points. The signal function is also described by the MC-simulated shape convolved with a Gaussian function, and the background function is described by a third-order Chebyshev polynomials. Figure 2(c) shows the fit result.

JHEP12(2022)153

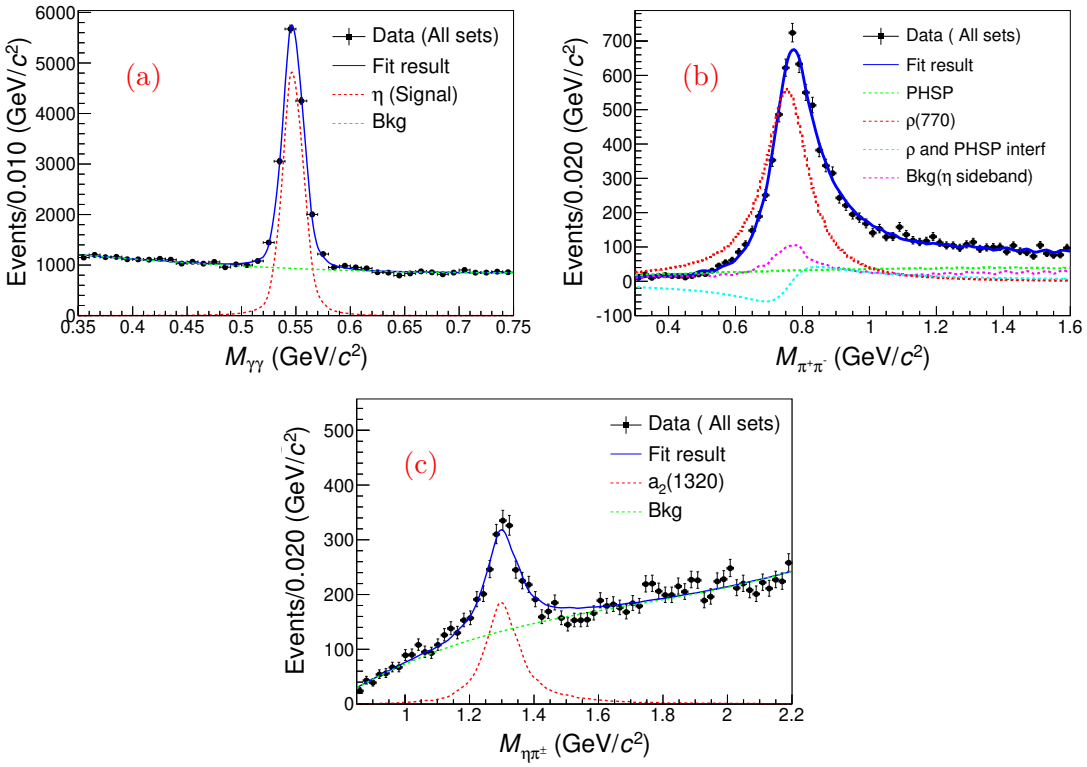

Figure 2. Fit result of (a) $M_{\gamma\gamma}$, (b) $M_{\pi^+\pi^-}$ and (c) $M_{\eta\pi^\pm}$ with the sum of all energy points. The points with error bars are data, the blue solid lines represent the total fit, the red dotted lines represent the signal components, the green dotted lines represent the background distribution, the cyan dotted line represent the interference between $\rho(770)$ and PHSP process and the pink dotted line represent the non-η background.

Source	$N_{\rm obs}$	ϵ (%)
$a_2^\pm(1320)\pi^\mp$	1526 $\pm$ 85	26.4
$\eta\rho^0$ + interference	6167 $\pm$ 76	24.9
$\eta\pi^+\pi^-$(3-body non-resonant)	4776 $\pm$ 181	27.2
$\eta\pi^+\pi^-$(total)	12469 $\pm$ 141	25.9

Table 1. The numerical results for each component summed over all energy points, while those for $N_{\rm obs}$ are statistical only. The number from $\eta\pi^+\pi^-$(total) is obtained by a fit to the $M_{\gamma\gamma}$. The uncertainty on the efficiencies for individual contributions is 0.2%, while below 0.1% for the $\eta\pi^+\pi^-$(total), which is negligible.

Numerical results for the fits for events summed over all energy points can be found in table 1. The number of $a_2^\pm(1320)\pi^\mp$ events is obtained by the fit to the $M_{\eta\pi^\pm}$ distribution, the number $\eta\rho^0$ + interference events is obtained by the fit to the $M_{\pi^+\pi^-}$ distribution, and number of $\eta\pi^+\pi^-$ (total) events is obtained by the fit to the $M_{\gamma\gamma}$ distribution. The number of events for the 3-body non-resonant process is given by $N(\eta\pi^+\pi^-$ (3-body non-resonant)) $= N(\eta\pi^+\pi^-$ (total)) $-$ N($\eta\rho^0$ + interference) $-$ N($a_2^\pm(1320)\pi^\mp$).

JHEP12(2022)153

6 Cross section calculation

The Born cross section at each energy point is calculated as:

$$\sigma^{\rm Born} = \frac{N_{\rm obs}}{\mathcal{L} \times \epsilon \times (1+\delta^{\gamma}) \times \frac{1}{|1-\Pi|^2} \times \mathcal{B}(\eta \to \gamma\gamma)}, \tag{6.1}$$

where $N_{\rm obs}$ is the number for observed signal events, $\mathcal{L}$ is the integrated luminosity, ϵ is the detection efficiency, and $1+\delta^{\gamma}$ and $\frac{1}{|1-\Pi|^2}$ are ISR and vacuum polarization (VP) factors, respectively. To obtain $1+\delta^{\gamma}$ and $\frac{1}{|1-\Pi|^2}$, we use an energy-dependent power function a/s^n as the initial input of the Born cross section, and the final one is obtained by iterating several times until the difference of $\epsilon \cdot (1+\delta^{\gamma})$ between the last two iterations is less than 1%. The relevant numbers related to the Born cross section measurement for $e^+e^- \to \eta\pi^+\pi^-$ and its intermediate process $e^+e^- \to \eta\rho^0$ are listed in tables 2 and 3, respectively. For the intermediate process $e^+e^- \to a_2(1320)^{\pm}\pi^{\mp}$, we do not report the measurement of its Born cross section due to the small event sample at single energy points.

7 Systematic uncertainty

The uncertainties in the Born cross section measurements include those of the luminosity measurement, tracking and PID efficiency, photon detection efficiency, branching fraction of intermediate decay, R ratio, E/cp ratio, decay depth in the μ counter, η mass window, J/ψ veto, fit of $M_{\gamma\gamma}$ and $M_{\pi^+\pi^-}$, intermediate state of $a_2(1320)$, kinematic fit, ISR and VP correction and detection efficiency.

- *Luminosity measurement*. The luminosity is measured using Bhabha events with uncertainty of 1.0% at all energy points [23, 24], which is taken as the systematic uncertainty from the luminosity measurement.

- *Tracking efficiency*. The pion tracking efficiency is determined by using the control sample $J/\psi \to p\bar{p}\pi^+\pi^-$. The difference between data and the MC simulation tracking efficiency is 1.0% per track [34].

- *PID efficiency*. The uncertainty related to the pion PID efficiency is studied with the sample $e^+e^- \to K^+K^-\pi^+\pi^-$, and the average difference of the PID efficiency between data and MC simulation is determined to be 1.0% for each charged pion, which is taken as the systematic uncertainty [35].

- *Photon detection efficiency*. The uncertainty caused by photon reconstruction is 1.0% per photon, which is studied by the control sample $J/\psi \to \gamma\pi^0\pi^0$ [36].

- *Branching fraction of intermediate decay*. The uncertainty due to the branching fraction $\mathcal{B}(\eta \to \gamma\gamma)$ is 0.5% from the PDG [28].

- *R ratio*. The uncertainty caused by the $R = \frac{|E_{\gamma_1} - E_{\gamma_2}|}{p_\eta}$ requirement is estimated by changing the range by +0.05 or −0.05. The larger differences with and without changes are taken as the corresponding uncertainties.

JHEP12(2022)153

$\sqrt{s}$ (GeV)	$\mathcal{L}_i$ (pb^{-1})	$N_{\rm obs}$	ϵ (%)	$1+\delta^\gamma$	$\frac{1}{\lvert 1-\Pi\rvert^2}$	$\sigma^{\rm Born}$ (pb)
3.872	219.2	244 ± 19	29.2	0.89	1.05	10.3 ± 0.8 ± 0.6
4.009	482.0	486 ± 27	25.2	0.94	1.04	10.3 ± 0.6 ± 0.6
4.130	401.5	361 ± 23	27.7	0.98	1.05	8.0 ± 0.5 ± 0.4
4.160	408.7	304 ± 22	27.5	0.98	1.05	6.7 ± 0.5 ± 0.4
4.180	3194.5	2649 ± 65	25.9	0.98	1.05	7.9 ± 0.2 ± 0.4
4.190	526.7	376 ± 25	26.5	0.99	1.06	6.6 ± 0.4 ± 0.4
4.200	526.0	412 ± 26	26.5	0.99	1.06	7.2 ± 0.4 ± 0.4
4.210	517.1	406 ± 24	26.2	0.99	1.06	7.2 ± 0.4 ± 0.4
4.220	514.6	415 ± 25	26.2	1.00	1.06	7.4 ± 0.5 ± 0.4
4.230	1056.4	811 ± 36	23.7	1.00	1.06	7.8 ± 0.3 ± 0.4
4.237	530.3	393 ± 25	26.2	1.00	1.06	6.8 ± 0.4 ± 0.4
4.246	538.1	385 ± 26	26.3	1.00	1.06	6.6 ± 0.4 ± 0.4
4.260	828.4	608 ± 31	23.5	1.01	1.05	7.5 ± 0.4 ± 0.4
4.270	531.1	377 ± 25	26.2	1.01	1.05	6.5 ± 0.4 ± 0.3
4.290	502.4	310 ± 22	26.6	1.00	1.05	5.6 ± 0.4 ± 0.3
4.315	501.2	320 ± 23	26.7	1.01	1.05	5.7 ± 0.4 ± 0.3
4.340	505.0	317 ± 23	26.6	1.02	1.05	5.6 ± 0.4 ± 0.3
4.360	543.9	342 ± 23	23.0	1.02	1.05	6.5 ± 0.4 ± 0.3
4.380	522.7	337 ± 24	26.5	1.03	1.05	5.7 ± 0.4 ± 0.3
4.400	507.8	298 ± 23	26.4	1.03	1.05	5.2 ± 0.4 ± 0.3
4.420	1043.9	579 ± 29	26.1	1.04	1.05	4.9 ± 0.2 ± 0.3
4.440	569.9	319 ± 23	26.3	1.04	1.05	4.9 ± 0.4 ± 0.3
4.600	586.9	245 ± 20	25.1	1.07	1.06	3.7 ± 0.3 ± 0.2
4.620	511.1	202 ± 21	25.7	1.07	1.05	3.5 ± 0.4 ± 0.2
4.640	541.4	227 ± 19	25.7	1.07	1.05	3.7 ± 0.3 ± 0.2
4.660	523.6	210 ± 19	25.5	1.08	1.05	3.5 ± 0.3 ± 0.2
4.680	1631.7	576 ± 31	25.5	1.08	1.05	3.1 ± 0.2 ± 0.2
4.700	526.2	193 ± 18	25.4	1.08	1.06	3.2 ± 0.3 ± 0.2

Table 2. Numerical results for $e^+e^- \to \eta\pi^+\pi^-$. The first uncertainties for cross sections in the most right column are statistical uncertainties and the second ones are systematic uncertainties, while those for $N_{\rm obs}$ are statistical only.

- *E/cp ratio*. The uncertainty caused by the E/cp ratio requirement is estimated from the control sample $J/\psi \to \pi^0\pi^+\pi^-$. The difference between data and MC simulation is found to be 3.9%, which is taken as the systematic uncertainty.

- *Decay depth in the μ counter*. The uncertainty caused by the requirement on the decay depth in the μ counter is estimated from the control sample $J/\psi \to \pi^0\pi^+\pi^-$. The difference between data and MC simulation is found to be 0.3% and is taken as the systematic uncertainty.

JHEP12(2022)153

$\sqrt{s}$ (GeV)	$\mathcal{L}_i$ (pb^{-1})	$N_{\rm obs}$	ϵ (%)	$1+\delta^{\gamma}$	$\frac{1}{\lvert 1-\Pi\rvert^2}$	$\sigma^{\rm Born}$ (pb)
3.872	219.2	125 ± 10	27.9	0.89	1.05	5.6 ± 0.5 ± 0.3
4.009	482.0	216 ± 13	25.2	0.95	1.04	4.6 ± 0.3 ± 0.3
4.130	401.5	178 ± 12	25.4	0.98	1.05	4.3 ± 0.3 ± 0.2
4.160	408.7	144 ± 11	25.4	0.99	1.05	3.4 ± 0.3 ± 0.2
4.180	3194.5	1287 ± 29	24.4	0.99	1.05	4.0 ± 0.1 ± 0.2
4.190	526.7	175 ± 12	24.8	1.00	1.06	3.2 ± 0.2 ± 0.2
4.200	526.0	198 ± 13	25.0	1.00	1.06	3.6 ± 0.2 ± 0.2
4.210	517.1	185 ± 12	24.5	1.00	1.06	3.5 ± 0.2 ± 0.2
4.220	514.6	204 ± 13	24.1	1.00	1.06	3.9 ± 0.2 ± 0.2
4.230	1056.4	382 ± 17	24.0	1.00	1.06	3.6 ± 0.2 ± 0.2
4.237	530.3	190 ± 12	24.3	1.01	1.06	3.5 ± 0.2 ± 0.2
4.246	538.1	189 ± 12	24.4	1.01	1.06	3.4 ± 0.2 ± 0.2
4.260	828.4	279 ± 15	23.5	1.01	1.05	3.4 ± 0.2 ± 0.2
4.270	531.1	191 ± 12	24.1	1.01	1.05	3.5 ± 0.2 ± 0.2
4.290	502.4	143 ± 11	24.0	1.02	1.05	2.8 ± 0.2 ± 0.2
4.315	501.2	163 ± 11	24.3	1.03	1.05	3.1 ± 0.2 ± 0.2
4.340	505.0	155 ± 11	23.9	1.03	1.05	3.0 ± 0.2 ± 0.2
4.360	543.9	157 ± 11	22.8	1.04	1.05	3.0 ± 0.2 ± 0.2
4.380	522.7	155 ± 11	23.7	1.05	1.05	2.9 ± 0.2 ± 0.2
4.400	507.8	132 ± 10	23.7	1.05	1.05	2.5 ± 0.2 ± 0.1
4.420	1043.9	265 ± 15	24.1	1.05	1.05	2.4 ± 0.1 ± 0.1
4.440	569.9	142 ± 11	23.7	1.06	1.05	2.4 ± 0.2 ± 0.1
4.600	586.9	107 ± 9	23.3	1.09	1.06	1.7 ± 0.2 ± 0.1
4.620	511.1	83 ± 8	22.5	1.10	1.05	1.6 ± 0.2 ± 0.1
4.640	541.4	108 ± 9	22.8	1.10	1.05	1.9 ± 0.2 ± 0.1
4.660	523.6	83 ± 8	22.5	1.10	1.05	1.5 ± 0.2 ± 0.1
4.680	1631.7	260 ± 13	22.8	1.10	1.05	1.5 ± 0.1 ± 0.1
4.700	526.2	72 ± 8	22.7	1.10	1.06	1.3 ± 0.1 ± 0.1

Table 3. Numerical results for $e^+e^- \to \eta\rho^0$. The first uncertainties for cross sections in the last column are statistical uncertainties and the second ones are systematic, while those for $N_{\rm obs}$ are statistical only.

- *η mass window.* The systematic uncertainty associated with the η mass window requirement is estimated by changing the mass window range by $+1\sigma$ or -1σ, where σ is the η mass resolution, the larger difference with and without change is taken as the systematic uncertainty.

- *J/ψ veto.* The systematic uncertainty from the J/ψ-related background veto is estimated by changing the J/ψ mass window from [3.05,3.15] GeV/c^2 to [3.06,3.14] or [3.04,3.16] GeV/c^2, and the larger difference with and without the change is taken as the systematic uncertainty.

JHEP12(2022)153

- *Fit of $M_{\gamma\gamma}$.* The systematic uncertainties associated with the fit of the $M_{\gamma\gamma}$ spectrum are caused by the background shape and fit range. They are estimated by changing the order of the Chebychev polynomial function from second to third and changing the fit range from [0.35, 0.75] GeV/c^2 to [0.40, 0.80] or [0.30, 0.70] GeV/c^2. The resulting differences with and without change are taken as the systematic uncertainties.

- *Fit of $M_{\pi^+\pi^-}$.* The systematic uncertainties associated with the fit of the $M_{\pi^+\pi^-}$ spectrum come from the choice of signal and background description and fit range. They are estimated by:

  – fixing the parameters of the BW function to the values from the PDG [28];
  – changing the order of the Chebychev polynomial function from second to third;
  – changing the fit range from [0.30, 1.60] GeV/c^2 to [0.35, 1.65] or [0.25, 1.55] GeV/c^2.

  The resulting differences with and without change are taken as the systematic uncertainties.

- *Intermediate state of $a_2(1320)$.* The intermediate state of $a_2(1320)$ signal yield is obtained from the fit to the $M_{\eta\pi^\pm}$ spectrum. The systematic uncertainty associated to the fit model is estimated by replacing the original model by the alternative one with additional factor accounting for the variation of the available phase space. As a result, though the number of $a_2(1320)$ signal candidates is changed by about 18%; the subsequent change of the cross-sections of the $\eta\pi^+\pi^-$ final state is found to be less than 0.1% for all energy points. Therefore, the corresponding uncertainty is neglected.

- *Kinematic fit.* The uncertainty due to the kinematic fit requirements is estimated by correcting the helix parameters of charged tracks according to the method described in ref. [37]. The difference between detection efficiencies obtained from MC samples with and without this correction is taken as the uncertainty. The uncertainties of the process $e^+e^- \to \eta\pi^+\pi^-$ are found to be less than 0.1% and are therefore neglected.

- *ISR and VP correction.* As mentioned in section 8, we use the energy-dependent power function $f(\sqrt{s}) = a/s^n$ to fit the line shape. The systematic uncertainty from the ISR and VP correction is estimated by varying the n value by $+1\sigma$ or -1σ, where σ is the statistical uncertainty of the fitted n value. The larger difference of the cross sections caused by the above changes is taken as the systematic uncertainty.

- *Detection efficiency.* The detection efficiency is obtained by a weighted average for the three different processes. The weight factors are the respective numbers of signal events. We randomly change the number of signal events for each process according to its statistical uncertainty and get new ratios between different processes. We mix the three processes with the new ratios and get new efficiencies. By repeating the above procedure, we obtain a group of detection efficiencies, which is almost a Gaussian distribution. The corresponding standard deviation is taken as the uncertainty caused by the detection efficiency. It is found to be less than 0.1% and is therefore neglected.

JHEP12(2022)153

$\sqrt{s}$ (GeV)	3.872	4.009	4.130	4.160	4.180	4.190	4.200	4.210	4.220	4.230	4.237	4.246	4.260	4.270
Luminosity measurement	1.0	1.0	1.0	1.0	1.0	1.0	1.0	1.0	1.0	1.0	1.0	1.0	1.0	1.0
Tracking efficiency	2.0	2.0	2.0	2.0	2.0	2.0	2.0	2.0	2.0	2.0	2.0	2.0	2.0	2.0
PID efficiency	2.0	2.0	2.0	2.0	2.0	2.0	2.0	2.0	2.0	2.0	2.0	2.0	2.0	2.0
Photon detection efficiency	2.0	2.0	2.0	2.0	2.0	2.0	2.0	2.0	2.0	2.0	2.0	2.0	2.0	2.0
Intermediate decay	0.5	0.5	0.5	0.5	0.5	0.5	0.5	0.5	0.5	0.5	0.5	0.5	0.5	0.5
R ratio	0.6	0.6	0.6	0.6	0.6	0.6	0.6	0.6	0.6	0.6	0.6	0.6	0.6	0.6
E/cp ratio	3.9	3.9	3.9	3.9	3.9	3.9	3.9	3.9	3.9	3.9	3.9	3.9	3.9	3.9
Decay depth in MuC	0.3	0.3	0.3	0.3	0.3	0.3	0.3	0.3	0.3	0.3	0.3	0.3	0.3	0.3
J/ψ veto	0.1	0.1	0.1	0.1	0.1	0.1	0.1	0.1	0.1	0.1	0.1	0.1	0.1	0.1
Fit range	0.2	0.0	0.1	0.1	0.1	0.1	0.1	0.1	0.1	0.1	0.1	0.1	0.1	0.1
Background shape	0.1	0.0	0.0	0.0	0.0	0.0	0.0	0.0	0.0	0.0	0.0	0.0	0.0	0.0
ISR and VP correction	0.4	0.4	0.1	0.5	0.8	0.9	0.7	0.7	0.5	0.1	0.2	0.8	0.2	0.4
Sum	5.4	5.4	5.4	5.4	5.4	5.4	5.4	5.4	5.4	5.4	5.4	5.4	5.4	5.4

$\sqrt{s}$ (GeV)	4.290	4.315	4.340	4.360	4.380	4.400	4.420	4.440	4.600	4.620	4.640	4.660	4.680	4.700
Luminosity measurement	1.0	1.0	1.0	1.0	1.0	1.0	1.0	1.0	1.0	1.0	1.0	1.0	1.0	1.0
Tracking efficiency	2.0	2.0	2.0	2.0	2.0	2.0	2.0	2.0	2.0	2.0	2.0	2.0	2.0	2.0
PID efficiency	2.0	2.0	2.0	2.0	2.0	2.0	2.0	2.0	2.0	2.0	2.0	2.0	2.0	2.0
Photon detection efficiency	2.0	2.0	2.0	2.0	2.0	2.0	2.0	2.0	2.0	2.0	2.0	2.0	2.0	2.0
Intermediate decay	0.5	0.5	0.5	0.5	0.5	0.5	0.5	0.5	0.5	0.5	0.5	0.5	0.5	0.5
R ratio	0.6	0.6	0.6	0.6	0.6	0.6	0.6	0.6	0.6	0.6	0.6	0.6	0.6	0.6
E/cp ratio	3.9	3.9	3.9	3.9	3.9	3.9	3.9	3.9	3.9	3.9	3.9	3.9	3.9	3.9
Decay depth in MuC	0.3	0.3	0.3	0.3	0.3	0.3	0.3	0.3	0.3	0.3	0.3	0.3	0.3	0.3
J/ψ veto	0.1	0.1	0.1	0.1	0.1	0.1	0.1	0.1	0.1	0.1	0.1	0.1	0.1	0.1
Fit range	0.1	0.1	0.1	0.1	0.1	0.1	0.1	0.1	0.1	0.1	0.1	0.1	0.1	0.0
Background shape	0.0	0.0	0.0	0.0	0.0	0.0	0.0	0.0	0.2	0.2	0.2	0.2	0.3	0.3
ISR and VP correction	0.8	0.5	0.8	0.2	0.5	0.2	0.5	0.5	0.4	0.8	1.2	0.8	0.8	1.0
Sum	5.4	5.4	5.4	5.4	5.4	5.4	5.4	5.4	5.4	5.4	5.5	5.4	5.4	5.5

Table 4. The relative systematic uncertainties (%) for the process $e^+e^- \to \eta\pi^+\pi^-$.

Due to the limited sample size at other c.m. energies, the systematic uncertainties from the event selection, mass window requirement and background veto are taken to be the same as those at $\sqrt{s} = 4.180\,\text{GeV}$. The total uncertainty in the cross section measurement is obtained by summing the individual contributions in quadrature, and the dominant uncertainties come from the tracking efficiency, PID efficiency, photon efficiency and E/cp ratio requirement. Systematic uncertainties are summarized in tables 4 and 5 for the processes $e^+e^- \to \eta\pi^+\pi^-$ and $e^+e^- \to \eta\rho$, respectively.

8 Fit to the Born cross sections

The least-squares method is used to fit the Born cross sections under different assumptions. In order to describe purely continuum production, we use the empirical energy-dependent function

$$f_1(\sqrt{s}) = a/s^n \tag{8.1}$$

JHEP12(2022)153

$\sqrt{s}$ (GeV)	3.872	4.009	4.130	4.160	4.180	4.190	4.200	4.210	4.220	4.230	4.237	4.246	4.260	4.270
Luminosity measurement	1.0	1.0	1.0	1.0	1.0	1.0	1.0	1.0	1.0	1.0	1.0	1.0	1.0	1.0
Tracking efficiency	2.0	2.0	2.0	2.0	2.0	2.0	2.0	2.0	2.0	2.0	2.0	2.0	2.0	2.0
PID efficiency	2.0	2.0	2.0	2.0	2.0	2.0	2.0	2.0	2.0	2.0	2.0	2.0	2.0	2.0
Photon detection efficiency	2.0	2.0	2.0	2.0	2.0	2.0	2.0	2.0	2.0	2.0	2.0	2.0	2.0	2.0
Intermediate decay	0.5	0.5	0.5	0.5	0.5	0.5	0.5	0.5	0.5	0.5	0.5	0.5	0.5	0.5
R ratio	0.3	0.3	0.3	0.3	0.3	0.3	0.3	0.3	0.3	0.3	0.3	0.3	0.3	0.3
E/cp ratio	3.9	3.9	3.9	3.9	3.9	3.9	3.9	3.9	3.9	3.9	3.9	3.9	3.9	3.9
η Mass Window	0.3	0.3	0.3	0.3	0.3	0.3	0.3	0.3	0.3	0.3	0.3	0.3	0.3	0.3
Fit range	0.3	0.1	0.0	0.0	0.0	0.0	0.0	0.0	0.0	0.0	0.0	0.0	0.0	0.0
Background shape	0.3	0.3	0.3	0.3	0.3	0.3	0.3	0.3	0.3	0.3	0.3	0.3	0.3	0.3
Signal shape	1.0	1.0	1.0	1.0	1.0	1.0	1.0	1.0	1.1	1.0	1.0	1.0	1.0	0.9
Kinematic fit	0.4	0.6	0.8	0.8	0.8	0.8	0.8	0.8	0.8	0.8	0.8	0.8	0.8	0.8
ISR and VP correction	0.1	0.1	0.1	0.2	0.4	0.2	0.1	0.2	0.2	0.4	0.4	0.5	0.2	0.5
Sum	5.5	5.5	5.5	5.5	5.5	5.5	5.5	5.5	5.5	5.5	5.5	5.5	5.5	5.5

$\sqrt{s}$ (GeV)	4.290	4.315	4.340	4.360	4.380	4.400	4.420	4.440	4.600	4.620	4.640	4.660	4.680	4.700
Luminosity measurement	1.0	1.0	1.0	1.0	1.0	1.0	1.0	1.0	1.0	1.0	1.0	1.0	1.0	1.0
Tracking efficiency	2.0	2.0	2.0	2.0	2.0	2.0	2.0	2.0	2.0	2.0	2.0	2.0	2.0	2.0
PID efficiency	2.0	2.0	2.0	2.0	2.0	2.0	2.0	2.0	2.0	2.0	2.0	2.0	2.0	2.0
Photon detection efficiency	2.0	2.0	2.0	2.0	2.0	2.0	2.0	2.0	2.0	2.0	2.0	2.0	2.0	2.0
Intermediate decay	0.5	0.5	0.5	0.5	0.5	0.5	0.5	0.5	0.5	0.5	0.5	0.5	0.5	0.5
R ratio	0.3	0.3	0.3	0.3	0.3	0.3	0.3	0.3	0.3	0.3	0.3	0.3	0.3	0.3
E/cp ratio	3.9	3.9	3.9	3.9	3.9	3.9	3.9	3.9	3.9	3.9	3.9	3.9	3.9	3.9
η Mass Window	0.3	0.3	0.3	0.3	0.3	0.3	0.3	0.3	0.3	0.3	0.3	0.3	0.3	0.3
Fit range	0.0	0.0	0.0	0.0	0.0	0.0	0.0	0.0	0.2	0.2	0.3	0.3	0.3	0.4
Background shape	0.3	0.3	0.3	0.3	0.3	0.3	0.3	0.3	0.3	0.3	0.3	0.3	0.3	0.3
Signal shape	0.9	0.9	1.0	1.1	1.0	1.0	1.0	1.0	1.0	0.9	1.0	0.9	1.0	0.8
Kinematic fit	0.8	0.8	0.8	0.8	0.8	0.8	0.8	0.8	0.6	0.6	0.5	0.5	0.5	0.4
ISR and VP correction	0.8	0.2	0.5	0.4	0.5	0.5	0.2	0.5	0.9	0.4	0.6	0.5	0.7	0.9
Sum	5.5	5.5	5.5	5.5	5.5	5.5	5.5	5.5	5.6	5.5	5.5	5.5	5.5	5.5

Table 5. The relative systematic uncertainties (%) for the process $e^+e^- \to \eta\rho^0$.

to fit the Born cross section which only considers the contribution from the one photon exchange process without any resonance contribution. The goodness-of-fit (GOF) is $\chi^2/\text{n.d.f.} = 47.0/27 = 1.7$ for the $\eta\pi^+\pi^-$ process and $47.5/27 = 1.8$ for the $\eta\rho$ process. Here, n.d.f. denotes the number of degrees of freedom. The χ^2 function is constructed as

$$\chi^2 = \sum \frac{(\sigma_{D_i} - \sigma_{D_i}^{\text{fit}})^2}{\delta_i^2}. \tag{8.2}$$

Here, σ_{D_i} and $\sigma_{D_i}^{\text{fit}}$ are the measured and fitted Born cross sections of the ith energy point, respectively, and δ_i is the standard deviation of the measured cross section, which includes the statistical uncertainties only. The goodness of the fits indicates that the data can be described by the energy-dependent function. The fit returns $n = 3.5 \pm 0.1$ and 3.8 ± 0.1 for the processes $\eta\pi^+\pi^-$ and $\eta\rho$, respectively. The fit results are shown in figure 3. Potential contributions from the well-established conventional charmonium states ψ or charmonium-like states Y, i.e. $\psi(4160)$, $Y(4230)$, $Y(4360)$, $\psi(4415)$, and $Y(4660)$, are investigated by

JHEP12(2022)153

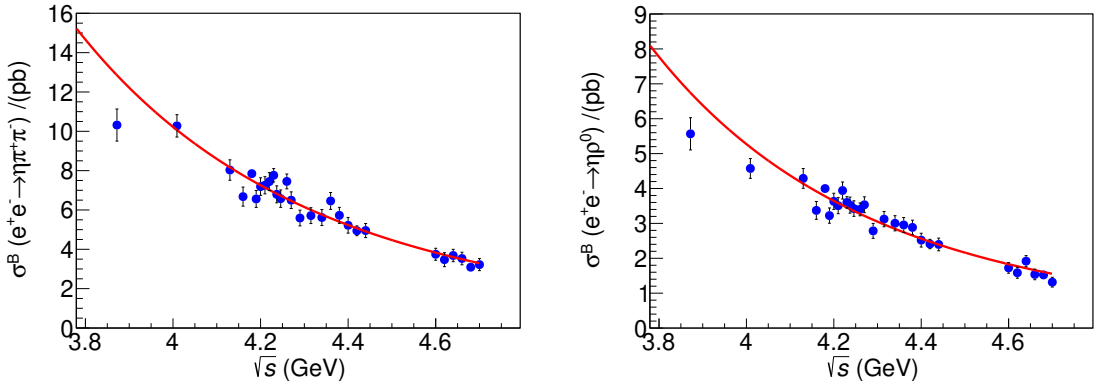

Figure 3. Fit to the Born cross section with function a/s^n (left) for the $e^+e^- \to \eta\pi^+\pi^-$ process and (right) for the $e^+e^- \to \eta\rho$ process. Here, the blue dots with error bars are the measured Born cross sections, and the red solid lines show the fit results.

using the coherent sum of the continuum (eq. (8.1)) and an additional charmonium(-like) state amplitude in the fit to the Born cross section. The fit function can be expressed as

$$\sigma(\sqrt{s}) = \left| f_1(\sqrt{s}) + \mathrm{BW}(\sqrt{s}) \left(\frac{\mathrm{PS}(\sqrt{s})}{\mathrm{PS}(M)} \right)^{1/2} e^{i\phi} \right|^2 , \tag{8.3}$$

where the parameters a and n in $f_1(\sqrt{s})$ are fixed to those obtained from the fit to the line shape using the function $f_1(\sqrt{s})$ only. The function $\mathrm{BW}(\sqrt{s}) = \frac{\sqrt{12\pi\Gamma_{ee}\mathcal{B}\Gamma_{\rm tot}}}{s-M^2+iM\Gamma_{\rm tot}^2}$ is used to describe charmonium(-like) states, where M, $\mathcal{B}$, Γ_{ee}, and $\Gamma_{\rm tot}$ are the mass, branching fraction of the resonance decays, partial width to e^+e^- and total width, respectively, in which Γ_{ee} and $\mathcal{B}$ are left free while the other two parameters are fixed to the values from the PDG [28], and $\frac{\mathrm{PS}(\sqrt{s})}{\mathrm{PS}(M)}$ is the three-body phase-space factor.

The statistical significances for the added components are estimated by comparing the change of χ^2/n.d.f. with and without adding the corresponding component. Since there is interference between the resonance and continuum process, there are two solutions for $\Gamma_{ee}\mathcal{B}(\eta\pi^+\pi^-/\eta\rho)$ with the same minimum value of χ^2. Table 6 lists the fit results and the significances for the additional charmonia. The low significances indicate that no charmonium or charmonium-like states are required to describe the measured cross section.

9 Summary

The processes of $e^+e^- \to \eta\pi^+\pi^-$ and $e^+e^- \to \eta\rho^0$ are studied at twenty-eight c.m. energies in the energy region from 3.872 to 4.700 GeV. The Born cross sections are obtained for all energy points. The lineshape of the Born cross section can be well described by the empirical exponential function eq. (8.1). The significances for possible contributions from $\psi(4160)$, $Y(4230)$, $Y(4360)$, $\psi(4415)$ or $Y(4660)$ resonances are all less than 2σ. This indicates a relatively small contribution from these resonances to the $\eta\pi^+\pi^-$ and $\eta\rho^0$ final states. More exploration of light hadron decay modes will be essential for a further understanding of the charmonium(-like) states.

JHEP12(2022)153

Channel	Resonance	$\Gamma_{ee}\mathcal{B}$ (eV) Solution I	$\Gamma_{ee}\mathcal{B}$ (eV) Solution II	Significance (σ)
$\eta\pi^+\pi^-$	$\psi(4160)$	$(7.4 \pm 1.6)\times10^{-4}$	$(9.6 \pm 0.1)\times10^{-1}$	1.1
	$Y(4230)$	$(5.4 \pm 3.4)\times10^{-4}$	$(7.6 \pm 0.1)\times10^{-1}$	1.6
	$Y(4360)$	$(6.8 \pm 2.9)\times10^{-4}$	$(10.9 \pm 0.2)\times10^{-1}$	0.6
	$\psi(4415)$	$(7.8 \pm 1.8)\times10^{-4}$	$(6.4 \pm 0.1)\times10^{-1}$	0.7
	$Y(4660)$	$(5.4 \pm 2.2)\times10^{-4}$	$(5.2 \pm 0.2)\times10^{-1}$	0.5
$\eta\rho^0$	$\psi(4160)$	$(4.4 \pm 1.5)\times10^{-4}$	$(4.8 \pm 0.1)\times10^{-1}$	1.0
	$Y(4230)$	$(2.4 \pm 1.0)\times10^{-4}$	$(3.8 \pm 0.1)\times10^{-1}$	1.1
	$Y(4360)$	$(9.1 \pm 1.1)\times10^{-4}$	$(5.4 \pm 0.1)\times10^{-1}$	1.6
	$\psi(4415)$	$(7.5 \pm 2.1)\times10^{-4}$	$(3.1 \pm 0.1)\times10^{-1}$	1.5
	$Y(4660)$	$(3.2 \pm 1.1)\times10^{-4}$	$(2.5 \pm 0.1)\times10^{-1}$	0.5

Table 6. Results of the fits to the Born cross section. Solution I represents the constructive solution, and Solution II represents the destructive solution.

Acknowledgments

The BESIII collaboration thanks the staff of BEPCII and the IHEP computing center for their strong support. This work is supported in part by National Key R&D Program of China under Contracts Nos. 2020YFA0406300, 2020YFA0406400; National Natural Science Foundation of China (NSFC) under Contracts Nos. 11805037, 11635010, 11735014, 11835012, 11935015, 11935016, 11935018, 11961141012, 12022510, 12025502, 12035009, 12035013, 12192260, 12192261, 12192262, 12192263, 12192264, 12192265; the Chinese Academy of Sciences (CAS) Large-Scale Scientific Facility Program; Joint Large-Scale Scientific Facility Funds of the NSFC and CAS under Contract No. U1832121, U1832207; 100 Talents Program of CAS; The Institute of Nuclear and Particle Physics (INPAC) and Shanghai Key Laboratory for Particle Physics and Cosmology; ERC under Contract No. 758462; European Union's Horizon 2020 research and innovation programme under Marie Sklodowska-Curie grant agreement under Contract No. 894790; German Research Foundation DFG under Contracts Nos. 443159800, Collaborative Research Center CRC 1044, GRK 2149; Istituto Nazionale di Fisica Nucleare, Italy; Ministry of Development of Turkey under Contract No. DPT2006K-120470; National Science and Technology fund; National Science Research and Innovation Fund (NSRF) via the Program Management Unit for Human Resources & Institutional Development, Research and Innovation under Contract No. B16F640076; STFC (United Kingdom); Suranaree University of Technology (SUT), Thailand Science Research and Innovation (TSRI), and National Science Research and Innovation Fund (NSRF) under Contract No. 160355; The Royal Society, U.K. under Contracts Nos. DH140054, DH160214; The Swedish Research Council; U.S. Department of Energy under Contract No. DE-FG02-05ER41374

JHEP12(2022)153

References

[1] Belle collaboration, *Observation of a narrow charmoniumlike state in exclusive $B^{\pm} \to K^{\pm}\pi^{+}\pi^{-}J/\psi$ decays*, *Phys. Rev. Lett.* **91** (2003) 262001 [hep-ex/0309032] [INSPIRE].

[2] BaBar collaboration, *Observation of a broad structure in the $\pi^{+}\pi^{-}J/\psi$ mass spectrum around 4.26 GeV/c^2*, *Phys. Rev. Lett.* **95** (2005) 142001 [hep-ex/0506081] [INSPIRE].

[3] BESIII collaboration, *Observation of a charged charmoniumlike structure in $e^{+}e^{-} \to \pi^{+}\pi^{-}J/\psi$ at $\sqrt{s} = 4.26$ GeV*, *Phys. Rev. Lett.* **110** (2013) 252001 [arXiv:1303.5949] [INSPIRE].

[4] Belle collaboration, *Study of $e^{+}e^{-} \to \pi^{+}\pi^{-}J/\psi$ and observation of a charged charmoniumlike state at Belle*, *Phys. Rev. Lett.* **110** (2013) 252002 [*Erratum ibid.* **111** (2013) 019901] [arXiv:1304.0121] [INSPIRE].

[5] CLEO collaboration, *Charmonium decays of $Y(4260)$, $\psi(4160)$ and $\psi(4040)$*, *Phys. Rev. Lett.* **96** (2006) 162003 [hep-ex/0602034] [INSPIRE].

[6] Belle collaboration, *Measurement of the $e^{+}e^{-} \to \pi^{+}\pi^{-}J/\psi$ cross section via initial-state radiation at Belle*, *Phys. Rev. Lett.* **99** (2007) 182004 [arXiv:0707.2541] [INSPIRE].

[7] BESIII collaboration, *Precise measurement of the $e^{+}e^{-} \to \pi^{+}\pi^{-}J/\psi$ cross section at center-of-mass energies from 3.77 to 4.60 GeV*, *Phys. Rev. Lett.* **118** (2017) 092001 [arXiv:1611.01317] [INSPIRE].

[8] BESIII collaboration, *Study of $e^{+}e^{-} \to \omega\chi_{cJ}$ at center of mass energies from 4.21 to 4.42 GeV*, *Phys. Rev. Lett.* **114** (2015) 092003 [arXiv:1410.6538] [INSPIRE].

[9] BESIII collaboration, *Precise measurement of the $e^{+}e^{-} \to \pi^{+}\pi^{-}J/\psi$ cross section at center-of-mass energies from 3.77 to 4.60 GeV*, *Phys. Rev. Lett.* **118** (2017) 092001 [arXiv:1611.01317] [INSPIRE].

[10] BESIII collaboration, *Measurement of $e^{+}e^{-} \to \pi^{+}\pi^{-}\psi(3686)$ from 4.008 to 4.600 GeV and observation of a charged structure in the $\pi^{\pm}\psi(3686)$ mass spectrum*, *Phys. Rev. D* **96** (2017) 032004 [*Erratum ibid.* **99** (2019) 019903] [arXiv:1703.08787] [INSPIRE].

[11] BESIII collaboration, *Evidence of a resonant structure in the $e^{+}e^{-} \to \pi^{+}D^{0}D^{*-}$ cross section between 4.05 and 4.60 GeV*, *Phys. Rev. Lett.* **122** (2019) 102002 [arXiv:1808.02847] [INSPIRE].

[12] F.E. Close and P.R. Page, *Gluonic charmonium resonances at BaBar and Belle?*, *Phys. Lett. B* **628** (2005) 215 [hep-ph/0507199] [INSPIRE].

[13] S. Dubynskiy and M.B. Voloshin, *Hadro-charmonium*, *Phys. Lett. B* **666** (2008) 344 [arXiv:0803.2224] [INSPIRE].

[14] BESIII collaboration, *Measurements of $e^{+}e^{-} \to K^{0}_{S}K^{\pm}\pi^{\mp}\pi^{0}$ and $e^{+}e^{-} \to K^{0}_{S}K^{\pm}\pi^{\mp}\eta$ at center-of-mass energies from 3.90 to 4.60 GeV*, *Phys. Rev. D* **99** (2019) 012003 [arXiv:1810.09395] [INSPIRE].

JHEP12(2022)153

[15] BESIII collaboration, *Precision measurements of the $e^+e^- \to K^0_S K^\pm \pi^\mp$ Born cross sections at center-of-mass energies between 3.8 and 4.6 GeV*, *Phys. Rev. D* **99** (2019) 072005 [arXiv:1808.08733] [INSPIRE].

[16] BESIII collaboration, *First measurement of $e^+e^- \to pK^0_S\bar{n}K^- + c.c.$ above open charm threshold*, *Phys. Rev. D* **98** (2018) 032014 [arXiv:1807.03468] [INSPIRE].

[17] BESIII collaboration, *Measurements of cross section of $e^+e^- \to \bar{p}p\pi^0$ at center-of-mass energies between 4.008 and 4.600 GeV*, *Phys. Lett. B* **771** (2017) 45 [arXiv:1701.04198] [INSPIRE].

[18] BESIII collaboration, *Design and construction of the BESIII detector*, *Nucl. Instrum. Meth. A* **614** (2010) 345 [arXiv:0911.4960] [INSPIRE].

[19] X. Li et al., *Study of MRPC technology for BESIII endcap-TOF upgrade*, *Radiat. Detect. Technol. Methods* **1** (2017) 13.

[20] Y.-X. Guo et al., *The study of time calibration for upgraded end cap TOF of BESIII*, *Radiat. Detect. Technol. Methods***1** (2017) 15.

[21] BESIII collaboration, *Measurements of the center-of-mass energies at BESIII via the di-muon process*, *Chin. Phys. C* **40** (2016) 063001 [arXiv:1510.08654] [INSPIRE].

[22] BESIII collaboration, *Measurements of the center-of-mass energies of e^+e^- collisions at BESIII*, *Chin. Phys. C* **45** (2021) 103001 [arXiv:2012.14750] [INSPIRE].

[23] BESIII collaboration, *Precision measurement of the integrated luminosity of the data taken by BESIII at center-of-mass energies between 3.810 GeV and 4.600 GeV*, *Chin. Phys. C* **39** (2015) 093001 [arXiv:1503.03408] [INSPIRE].

[24] BESIII collaboration, *Measurement of integrated luminosities at BESIII for data samples at center-of-mass energies between 4.0 and 4.6 GeV*, *Chin. Phys. C* **46** (2022) 113002 [arXiv:2203.03133] [INSPIRE].

[25] GEANT4 collaboration, *Geant4 — a simulation toolkit*, *Nucl. Instrum. Meth. A* **506** (2003) 250 [INSPIRE].

[26] S. Jadach, B.F.L. Ward and Z. Was, *Coherent exclusive exponentiation for precision Monte Carlo calculations*, *Phys. Rev. D* **63** (2001) 113009 [hep-ph/0006359] [INSPIRE].

[27] R.-G. Ping, *Event generators at BESIII*, *Chin. Phys. C* **32** (2008) 599 [INSPIRE].

[28] Particle Data Group collaboration, *Review of particle physics*, *PTEP* **2020** (2020) 083C01 [INSPIRE].

[29] J.C. Chen, G.S. Huang, X.R. Qi, D.H. Zhang and Y.S. Zhu, *Event generator for J/ψ and $\psi(2S)$ decay*, *Phys. Rev. D* **62** (2000) 034003 [INSPIRE].

[30] E. Richter-Was, *QED bremsstrahlung in semileptonic B and leptonic τ decays*, *Phys. Lett. B* **303** (1993) 163 [INSPIRE].

[31] S. Holz et al., *Towards an improved understanding of $\eta \to \gamma^*\gamma^*$*, *Eur. Phys. J. C* **81** (2021) 1002 [arXiv:1509.02194] [INSPIRE].

[32] X.Y. Zhou, S.X. Du, G. Li and C.P. Shen, *TopoAna: A generic tool for the event type analysis of inclusive Monte-Carlo samples in high energy physics experiments*, *Comput. Phys. Commun.* **258** (2021) 107540 [INSPIRE].

[33] BESIII collaboration, *Study of J/ψ and $\psi(3686)$ decays to $\pi^+\pi^-\eta'$*, *Phys. Rev. D* **96** (2017) 112012 [arXiv:1709.00018] [INSPIRE].

JHEP12(2022)153

[34] W.-L. Yuan et al., *Study of tracking efficiency and its systematic uncertainty from $J/\psi \to p\bar{p}\pi^+\pi^-$ at BESIII*, *Chin. Phys. C* **40** (2016) 026201 [arXiv:1507.03453] [INSPIRE].

[35] BESIII collaboration, *Search for a strangeonium-like structure Z_s decaying into $\phi\pi$ and a measurement of the cross section $e^+e^- \to \phi\pi\pi$*, *Phys. Rev. D* **99** (2019) 011101 [arXiv:1801.10384] [INSPIRE].

[36] BESIII collaboration, *Amplitude analysis of the $\pi^0\pi^0$ system produced in radiative J/ψ decays*, *Phys. Rev. D* **92** (2015) 052003 [*Erratum ibid.* **93** (2016) 039906] [arXiv:1506.00546] [INSPIRE].

[37] BESIII collaboration, *Search for hadronic transition $\chi_{cJ} \to \eta_c\pi^+\pi^-$ and observation of $\chi_{cJ} \to K\bar{K}\pi\pi\pi$*, *Phys. Rev. D* **87** (2013) 012002 [arXiv:1208.4805] [INSPIRE].

JHEP12(2022)153

The BESIII collaboration

M. Ablikim[1], M.N. Achasov[11,b], P. Adlarson[70], M. Albrecht[4], R. Aliberti[31], A. Amoroso[69A,69C], M.R. An[35], Q. An[66,53], X.H. Bai[61], Y. Bai[52], O. Bakina[32], R. Baldini Ferroli[26A], I. Balossino[27A], Y. Ban[42,g], V. Batozskaya[1,40], D. Becker[31], K. Begzsuren[29], N. Berger[31], M. Bertani[26A], D. Bettoni[27A], F. Bianchi[69A,69C], J. Bloms[63], A. Bortone[69A,69C], I. Boyko[32], R.A. Briere[5], A. Brueggemann[63], H. Cai[71], X. Cai[1,53], A. Calcaterra[26A], G.F. Cao[1,58], N. Cao[1,58], S.A. Cetin[57A], J.F. Chang[1,53], W.L. Chang[1,58], G. Chelkov[32,a], C. Chen[39], Chao Chen[50], G. Chen[1], H.S. Chen[1,58], M.L. Chen[1,53], S.J. Chen[38], S.M. Chen[56], T. Chen[1], X.R. Chen[28,58], X.T. Chen[1], Y.B. Chen[1,53], Z.J. Chen[23,h], W.S. Cheng[69C], S.K. Choi [50], X. Chu[39], G. Cibinetto[27A], F. Cossio[69C], J.J. Cui[45], H.L. Dai[1,53], J.P. Dai[73], A. Dbeyssi[17], R.E. de Boer[4], D. Dedovich[32], Z.Y. Deng[1], A. Denig[31], I. Denysenko[32], M. Destefanis[69A,69C], F. De Mori[69A,69C], Y. Ding[36], J. Dong[1,53], L.Y. Dong[1,58], M.Y. Dong[1,53,58], X. Dong[71], S.X. Du[75], P. Egorov[32,a], Y.L. Fan[71], J. Fang[1,53], S.S. Fang[1,58], W.X. Fang[1], Y. Fang[1], R. Farinelli[27A], L. Fava[69B,69C], F. Feldbauer[4], G. Felici[26A], C.Q. Feng[66,53], J.H. Feng[54], K Fischer[64], M. Fritsch[4], C. Fritzsch[63], C.D. Fu[1], H. Gao[58], Y.N. Gao[42,g], Yang Gao[66,53], S. Garbolino[69C], I. Garzia[27A,27B], P.T. Ge[71], Z.W. Ge[38], C. Geng[54], E.M. Gersabeck[62], A Gilman[64], K. Goetzen[12], L. Gong[36], W.X. Gong[1,53], W. Gradl[31], M. Greco[69A,69C], L.M. Gu[38], M.H. Gu[1,53], Y.T. Gu[14], C. Y Guan[1,58], A.Q. Guo[28,58], L.B. Guo[37], R.P. Guo[44], Y.P. Guo[10,f], A. Guskov[32,a], T.T. Han[45], W.Y. Han[35], X.Q. Hao[18], F.A. Harris[60], K.K. He[50], K.L. He[1,58], F.H. Heinsius[4], C.H. Heinz[31], Y.K. Heng[1,53,58], C. Herold[55], M. Himmelreich[31,d], G.Y. Hou[1,58], Y.R. Hou[58], Z.L. Hou[1], H.M. Hu[1,58], J.F. Hu[51,i], T. Hu[1,53,58], Y. Hu[1], G.S. Huang[66,53], K.X. Huang[54], L.Q. Huang[28,58], X.T. Huang[45], Y.P. Huang[1], Z. Huang[42,g], T. Hussain[68], N Hüsken[25,31], W. Imoehl[25], M. Irshad[66,53], J. Jackson[25], S. Jaeger[4], S. Janchiv[29], E. Jang[50], J.H. Jeong[50], Q. Ji[1], Q.P. Ji[18], X.B. Ji[1,58], X.L. Ji[1,53], Y.Y. Ji[45], Z.K. Jia[66,53], H.B. Jiang[45], S.S. Jiang[35], X.S. Jiang[1,53,58], Y. Jiang[58], J.B. Jiao[45], Z. Jiao[21], S. Jin[38], Y. Jin[61], M.Q. Jing[1,58], T. Johansson[70], N. Kalantar-Nayestanaki[59], X.S. Kang[36], R. Kappert[59], B.C. Ke[75], I.K. Keshk[4], A. Khoukaz[63], R. Kiuchi[1], R. Kliemt[12], L. Koch[33], O.B. Kolcu[57A], B. Kopf[4], M. Kuemmel[4], M. Kuessner[4], A. Kupsc[40,70], W. Kühn[33], J.J. Lane[62], J.S. Lange[33], P. Larin[17], A. Lavania[24], L. Lavezzi[69A,69C], Z.H. Lei[66,53], H. Leithoff[31], M. Lellmann[31], T. Lenz[31], C. Li[43], C. Li[39], C.H. Li[35], Cheng Li[66,53], D.M. Li[75], F. Li[1,53], G. Li[1], H. Li[47], H. Li[66,53], H.B. Li[1,58], H.J. Li[18], H.N. Li[51,i], J.Q. Li[4], J.S. Li[54], J.W. Li[45], Ke Li[1], L. J Li[1], L.K. Li[1], Lei Li[3], M.H. Li[39], P.R. Li[34,j,k], S.X. Li[10], S.Y. Li[56], T. Li[45], W.D. Li[1,58], W.G. Li[1], X.H. Li[66,53], X.L. Li[45], Xiaoyu Li[1,58], Z.X. Li[14], H. Liang[66,53], H. Liang[1,58], H. Liang[30], Y.F. Liang[49], Y.T. Liang[28,58], G.R. Liao[13], L.Z. Liao[45], J. Libby[24], A. Limphirat[55], C.X. Lin[54], D.X. Lin[28,58], T. Lin[1], B.J. Liu[1], C.X. Liu[1], D. Liu[17,66], F.H. Liu[48], Fang Liu[1], Feng Liu[6], G.M. Liu[51,i], H. Liu[34,j,k], H.B. Liu[14], H.M. Liu[1,58], Huanhuan Liu[1], Huihui Liu[19], J.B. Liu[66,53], J.L. Liu[67], J.Y. Liu[1,58], K. Liu[1], K.Y. Liu[36], Ke Liu[20], L. Liu[66,53], Lu Liu[39], M.H. Liu[10,f], P.L. Liu[1], Q. Liu[58], S.B. Liu[66,53], T. Liu[10,f], W.K. Liu[39], W.M. Liu[66,53], X. Liu[34,j,k], Y. Liu[34,j,k], Y.B. Liu[39], Z.A. Liu[1,53,58], Z.Q. Liu[45], X.C. Lou[1,53,58], F.X. Lu[54], H.J. Lu[21], J.G. Lu[1,53], X.L. Lu[1], Y. Lu[7], Y.P. Lu[1,53], Z.H. Lu[1], C.L. Luo[37], M.X. Luo[74], T. Luo[10,f], X.L. Luo[1,53], X.R. Lyu[58], Y.F. Lyu[39], F.C. Ma[36], H.L. Ma[1], L.L. Ma[45], M.M. Ma[1,58], Q.M. Ma[1], R.Q. Ma[1,58], R.T. Ma[58], X.Y. Ma[1,53], Y. Ma[42,g], F.E. Maas[17], M. Maggiora[69A,69C], S. Maldaner[4], S. Malde[64], Q.A. Malik[68], A. Mangoni[26B], Y.J. Mao[42,g], Z.P. Mao[1], S. Marcello[69A,69C], Z.X. Meng[61], G. Mezzadri[27A], H. Miao[1], T.J. Min[38], R.E. Mitchell[25], X.H. Mo[1,53,58], N. Yu. Muchnoi[11,b], Y. Nefedov[32], F. Nerling[17,d], I.B. Nikolaev[11,b], Z. Ning[1,53], S. Nisar[9,l], Y. Niu [45], S.L. Olsen[58], Q. Ouyang[1,53,58], S. Pacetti[26B,26C], X. Pan[10,f], Y. Pan[52], A. Pathak[30], M. Pelizaeus[4], H.P. Peng[66,53], K. Peters[12,d], J.L. Ping[37], R.G. Ping[1,58], S. Plura[31], S. Pogodin[32], V. Prasad[66,53], F.Z. Qi[1], H. Qi[66,53], H.R. Qi[56], M. Qi[38], T.Y. Qi[10,f], S. Qian[1,53], W.B. Qian[58], Z. Qian[54], C.F. Qiao[58], J.J. Qin[67], L.Q. Qin[13],

JHEP12(2022)153

X.P. Qin[10,f], X.S. Qin[45], Z.H. Qin[1,53], J.F. Qiu[1], S.Q. Qu[39], S.Q. Qu[56], K.H. Rashid[68], C.F. Redmer[31], K.J. Ren[35], A. Rivetti[69C], V. Rodin[59], M. Rolo[69C], G. Rong[1,58], Ch. Rosner[17], S.N. Ruan[39], H.S. Sang[66], A. Sarantsev[32,c], Y. Schelhaas[31], C. Schnier[4], K. Schoenning[70], M. Scodeggio[27A,27B], K.Y. Shan[10,f], W. Shan[22], X.Y. Shan[66,53], J.F. Shangguan[50], L.G. Shao[1,58], M. Shao[66,53], C.P. Shen[10,f], H.F. Shen[1,58], X.Y. Shen[1,58], B.A. Shi[58], H.C. Shi[66,53], J.Y. Shi[1], q. q. Shi[50], R.S. Shi[1,58], X. Shi[1,53], X. D Shi[66,53], J.J. Song[18], W.M. Song[30,1], Y.X. Song[42,g], S. Sosio[69A,69C], S. Spataro[69A,69C], F. Stieler[31], K.X. Su[71], P.P. Su[50], Y.J. Su[58], G.X. Sun[1], H. Sun[58], H.K. Sun[1], J.F. Sun[18], L. Sun[71], S.S. Sun[1,58], T. Sun[1,58], W.Y. Sun[30], X Sun[23,h], Y.J. Sun[66,53], Y.Z. Sun[1], Z.T. Sun[45], Y.H. Tan[71], Y.X. Tan[66,53], C.J. Tang[49], G.Y. Tang[1], J. Tang[54], L. Y Tao[67], Q.T. Tao[23,h], M. Tat[64], J.X. Teng[66,53], V. Thoren[70], W.H. Tian[47], Y. Tian[28,58], I. Uman[57B], B. Wang[1], B.L. Wang[58], C.W. Wang[38], D.Y. Wang[42,g], F. Wang[67], H.J. Wang[34,j,k], H.P. Wang[1,58], K. Wang[1,53], L.L. Wang[1], M. Wang[45], M.Z. Wang[42,g], Meng Wang[1,58], S. Wang[13], S. Wang[10,f], T. Wang[10,f], T.J. Wang[39], W. Wang[54], W.H. Wang[71], W.P. Wang[66,53], X. Wang[42,g], X.F. Wang[34,j,k], X.L. Wang[10,f], Y. Wang[56], Y.D. Wang[41], Y.F. Wang[1,53,58], Y.H. Wang[43], Y.Q. Wang[1], Yaqian Wang[16,1], Z. Wang[1,53], Z.Y. Wang[1,58], Ziyi Wang[58], D.H. Wei[13], F. Weidner[63], S.P. Wen[1], D.J. White[62], U. Wiedner[4], G. Wilkinson[64], M. Wolke[70], L. Wollenberg[4], J.F. Wu[1,58], L.H. Wu[1], L.J. Wu[1,58], X. Wu[10,f], X.H. Wu[30], Y. Wu[66], Z. Wu[1,53], L. Xia[66,53], T. Xiang[42,g], D. Xiao[34,j,k], G.Y. Xiao[38], H. Xiao[10,f], S.Y. Xiao[1], Y.L. Xiao[10,f], Z.J. Xiao[37], C. Xie[38], X.H. Xie[42,g], Y. Xie[45], Y.G. Xie[1,53], Y.H. Xie[6], Z.P. Xie[66,53], T.Y. Xing[1,58], C.F. Xu[1], C.J. Xu[54], G.F. Xu[1], H.Y. Xu[61], Q.J. Xu[15], X.P. Xu[50], Y.C. Xu[58], Z.P. Xu[38], F. Yan[10,f], L. Yan[10,f], W.B. Yan[66,53], W.C. Yan[75], H.J. Yang[46,e], H.L. Yang[30], H.X. Yang[1], L. Yang[47], S.L. Yang[58], Tao Yang[1], Y.F. Yang[39], Y.X. Yang[1,58], Yifan Yang[1,58], M. Ye[1,53], M.H. Ye[8], J.H. Yin[1], Z.Y. You[54], B.X. Yu[1,53,58], C.X. Yu[39], G. Yu[1,58], T. Yu[67], X.D. Yu[42,g], C.Z. Yuan[1,58], L. Yuan[2], S.C. Yuan[1], X.Q. Yuan[1], Y. Yuan[1,58], Z.Y. Yuan[54], C.X. Yue[35], A.A. Zafar[68], F.R. Zeng[45], X. Zeng[6], Y. Zeng[23,h], Y.H. Zhan[54], A.Q. Zhang[1], B.L. Zhang[1], B.X. Zhang[1], D.H. Zhang[39], G.Y. Zhang[18], H. Zhang[66], H.H. Zhang[30], H.H. Zhang[54], H.Y. Zhang[1,53], J.L. Zhang[72], J.Q. Zhang[37], J.W. Zhang[1,53,58], J.X. Zhang[34,j,k], J.Y. Zhang[1], J.Z. Zhang[1,58], Jianyu Zhang[1,58], Jiawei Zhang[1,58], L.M. Zhang[56], L.Q. Zhang[54], Lei Zhang[38], P. Zhang[1], Q.Y. Zhang[35,75], Shuihan Zhang[1,58], Shulei Zhang[23,h], X.D. Zhang[41], X.M. Zhang[1], X.Y. Zhang[45], X.Y. Zhang[50], Y. Zhang[64], Y.T. Zhang[75], Y.H. Zhang[1,53], Yan Zhang[66,53], Yao Zhang[1], Z.H. Zhang[1], Z.Y. Zhang[71], Z.Y. Zhang[39], G. Zhao[1], J. Zhao[35], J.Y. Zhao[1,58], J.Z. Zhao[1,53], Lei Zhao[66,53], Ling Zhao[1], M.G. Zhao[39], Q. Zhao[1], S.J. Zhao[75], Y.B. Zhao[1,53], Y.X. Zhao[28,58], Z.G. Zhao[66,53], A. Zhemchugov[32,a], B. Zheng[67], J.P. Zheng[1,53], Y.H. Zheng[58], B. Zhong[37], C. Zhong[67], X. Zhong[54], H. Zhou[45], L.P. Zhou[1,58], X. Zhou[71], X.K. Zhou[58], X.R. Zhou[66,53], X.Y. Zhou[35], Y.Z. Zhou[10,f], J. Zhu[39], K. Zhu[1], K.J. Zhu[1,53,58], L.X. Zhu[58], S.H. Zhu[65], S.Q. Zhu[38], T.J. Zhu[72], W.J. Zhu[10,f], Y.C. Zhu[66,53], Z.A. Zhu[1,58], B.S. Zou[1], J.H. Zou[1]

[1] *Institute of High Energy Physics, Beijing 100049, People's Republic of China*
[2] *Beihang University, Beijing 100191, People's Republic of China*
[3] *Beijing Institute of Petrochemical Technology, Beijing 102617, People's Republic of China*
[4] *Bochum Ruhr-University, D-44780 Bochum, Germany*
[5] *Carnegie Mellon University, Pittsburgh, Pennsylvania 15213, U.S.A.*
[6] *Central China Normal University, Wuhan 430079, People's Republic of China*
[7] *Central South University, Changsha 410083, People's Republic of China*
[8] *China Center of Advanced Science and Technology, Beijing 100190, People's Republic of China*
[9] *COMSATS University Islamabad, Lahore Campus, Defence Road, Off Raiwind Road, 54000 Lahore, Pakistan*
[10] *Fudan University, Shanghai 200433, People's Republic of China*
[11] *G.I. Budker Institute of Nuclear Physics SB RAS (BINP), Novosibirsk 630090, Russia*

JHEP12(2022)153

[12] GSI Helmholtzcentre for Heavy Ion Research GmbH, D-64291 Darmstadt, Germany
[13] Guangxi Normal University, Guilin 541004, People's Republic of China
[14] Guangxi University, Nanning 530004, People's Republic of China
[15] Hangzhou Normal University, Hangzhou 310036, People's Republic of China
[16] Hebei University, Baoding 071002, People's Republic of China
[17] Helmholtz Institute Mainz, Staudinger Weg 18, D-55099 Mainz, Germany
[18] Henan Normal University, Xinxiang 453007, People's Republic of China
[19] Henan University of Science and Technology, Luoyang 471003, People's Republic of China
[20] Henan University of Technology, Zhengzhou 450001, People's Republic of China
[21] Huangshan College, Huangshan 245000, People's Republic of China
[22] Hunan Normal University, Changsha 410081, People's Republic of China
[23] Hunan University, Changsha 410082, People's Republic of China
[24] Indian Institute of Technology Madras, Chennai 600036, India
[25] Indiana University, Bloomington, Indiana 47405, U.S.A.
[26] INFN Laboratori Nazionali di Frascati, (A)INFN Laboratori Nazionali di Frascati, I-00044, Frascati, Italy; (B)INFN Sezione di Perugia, I-06100, Perugia, Italy; (C)University of Perugia, I-06100, Perugia, Italy
[27] INFN Sezione di Ferrara, (A)INFN Sezione di Ferrara, I-44122, Ferrara, Italy; (B)University of Ferrara, I-44122, Ferrara, Italy
[28] Institute of Modern Physics, Lanzhou 730000, People's Republic of China
[29] Institute of Physics and Technology, Peace Avenue 54B, Ulaanbaatar 13330, Mongolia
[30] Jilin University, Changchun 130012, People's Republic of China
[31] Johannes Gutenberg University of Mainz, Johann-Joachim-Becher-Weg 45, D-55099 Mainz, Germany
[32] Joint Institute for Nuclear Research, 141980 Dubna, Moscow region, Russia
[33] Justus-Liebig-Universitaet Giessen, II. Physikalisches Institut, Heinrich-Buff-Ring 16, D-35392 Giessen, Germany
[34] Lanzhou University, Lanzhou 730000, People's Republic of China
[35] Liaoning Normal University, Dalian 116029, People's Republic of China
[36] Liaoning University, Shenyang 110036, People's Republic of China
[37] Nanjing Normal University, Nanjing 210023, People's Republic of China
[38] Nanjing University, Nanjing 210093, People's Republic of China
[39] Nankai University, Tianjin 300071, People's Republic of China
[40] National Centre for Nuclear Research, Warsaw 02-093, Poland
[41] North China Electric Power University, Beijing 102206, People's Republic of China
[42] Peking University, Beijing 100871, People's Republic of China
[43] Qufu Normal University, Qufu 273165, People's Republic of China
[44] Shandong Normal University, Jinan 250014, People's Republic of China
[45] Shandong University, Jinan 250100, People's Republic of China
[46] Shanghai Jiao Tong University, Shanghai 200240, People's Republic of China
[47] Shanxi Normal University, Linfen 041004, People's Republic of China
[48] Shanxi University, Taiyuan 030006, People's Republic of China
[49] Sichuan University, Chengdu 610064, People's Republic of China
[50] Soochow University, Suzhou 215006, People's Republic of China
[51] South China Normal University, Guangzhou 510006, People's Republic of China
[52] Southeast University, Nanjing 211100, People's Republic of China
[53] State Key Laboratory of Particle Detection and Electronics, Beijing 100049, Hefei 230026, People's Republic of China
[54] Sun Yat-Sen University, Guangzhou 510275, People's Republic of China
[55] Suranaree University of Technology, University Avenue 111, Nakhon Ratchasima 30000, Thailand
[56] Tsinghua University, Beijing 100084, People's Republic of China
[57] Turkish Accelerator Center Particle Factory Group, (A)Istinye University, 34010, Istanbul, Turkey; (B)Near East University, Nicosia, North Cyprus, Mersin 10, Turkey

JHEP12(2022)153

[58] University of Chinese Academy of Sciences, Beijing 100049, People's Republic of China
[59] University of Groningen, NL-9747 AA Groningen, The Netherlands
[60] University of Hawaii, Honolulu, Hawaii 96822, U.S.A.
[61] University of Jinan, Jinan 250022, People's Republic of China
[62] University of Manchester, Oxford Road, Manchester, M13 9PL, United Kingdom
[63] University of Muenster, Wilhelm-Klemm-Strasse 9, 48149 Muenster, Germany
[64] University of Oxford, Keble Road, Oxford OX13RH, United Kingdom
[65] University of Science and Technology Liaoning, Anshan 114051, People's Republic of China
[66] University of Science and Technology of China, Hefei 230026, People's Republic of China
[67] University of South China, Hengyang 421001, People's Republic of China
[68] University of the Punjab, Lahore-54590, Pakistan
[69] University of Turin and INFN, (A)University of Turin, I-10125, Turin, Italy; (B)University of Eastern Piedmont, I-15121, Alessandria, Italy; (C)INFN, I-10125, Turin, Italy
[70] Uppsala University, Box 516, SE-75120 Uppsala, Sweden
[71] Wuhan University, Wuhan 430072, People's Republic of China
[72] Xinyang Normal University, Xinyang 464000, People's Republic of China
[73] Yunnan University, Kunming 650500, People's Republic of China
[74] Zhejiang University, Hangzhou 310027, People's Republic of China
[75] Zhengzhou University, Zhengzhou 450001, People's Republic of China

[a] Also at the Moscow Institute of Physics and Technology, Moscow 141700, Russia
[b] Also at the Novosibirsk State University, Novosibirsk, 630090, Russia
[c] Also at the NRC "Kurchatov Institute", PNPI, 188300, Gatchina, Russia
[d] Also at Goethe University Frankfurt, 60323 Frankfurt am Main, Germany
[e] Also at Key Laboratory for Particle Physics, Astrophysics and Cosmology, Ministry of Education; Shanghai Key Laboratory for Particle Physics and Cosmology; Institute of Nuclear and Particle Physics, Shanghai 200240, People's Republic of China
[f] Also at Key Laboratory of Nuclear Physics and Ion-beam Application (MOE) and Institute of Modern Physics, Fudan University, Shanghai 200443, People's Republic of China
[g] Also at State Key Laboratory of Nuclear Physics and Technology, Peking University, Beijing 100871, People's Republic of China
[h] Also at School of Physics and Electronics, Hunan University, Changsha 410082, China
[i] Also at Guangdong Provincial Key Laboratory of Nuclear Science, Institute of Quantum Matter, South China Normal University, Guangzhou 510006, China
[j] Also at Frontiers Science Center for Rare Isotopes, Lanzhou University, Lanzhou 730000, People's Republic of China
[k] Also at Lanzhou Center for Theoretical Physics, Lanzhou University, Lanzhou 730000, People's Republic of China
[l] Also at the Department of Mathematical Sciences, IBA, Karachi, Pakistan

JHEP12(2022)153